# Mach-Zehnder Interferometer on a Silicon Photonic Integrated Chip

Chetan Sriram Madasu (edX: MChetanSR), chetan.madasu@gmail.com

## I. Introduction

The Mach-Zehnder interferometer (MZI) is an optical device that measures phase difference between two paths in free space or in optical media. It is an essential tool in precision applications such as metrology, quantum computing/information, and telecommunications. It consists of two beam splitters and two mirrors arranged in a way that splits an incoming beam of light into two separate paths, which later recombine after traversing a region of interest. Any differences in the optical path length cause interference that produces an intensity pattern that is indicative of variations in refractive index, temperature, or movement in the region of interest. This interferometer is widely used in experimental physics and engineering, particularly in precision measurements and quantum optics.

In this paper, we propose designs of MZI on a photonic integrated chip (PIC) that is used as a design case study for directing light through passive elements such as waveguides, grating couplers and Y-braches made of Si deposited on $SiO_2$ substrate. We briefly introduce the theory of the MZI, simulate its constituent passives with numerical tools. We also prepare the fabrication layout of the proposed MZIs using open-source tools. The layout is then fabricated and measured to characterize free spectral range. We measure the group refractive index of a silicon waveguide within a specific measurement bandwidth and quantitatively compare the results with simulations.

## II. Theory

The architecture of MZI in PIC is slightly different from that in free space. In PIC, the input light is split into two approximately equal parts using a Y-branch, then allowed to propagate in two different waveguides before combining the two fields using a Y-combiner. The beam splitter and mirrors used to direct the light in free space MZI are replaced by Y-branch and waveguides, respectively.

If we consider the electric field through different components of the MZI in an ideal scenario without loss mechanisms and dispersion, we end up with same expression for the transmission as in the case of a free-space MZI. This transmission for a $\Delta\phi$ phase difference between the two arms of the MZI reads,

$$\begin{aligned}\frac{I_o}{I_i} &= \frac{1}{2}(1+\cos(\Delta\phi)) \\ &= \frac{1}{2}(1+\cos(\beta\Delta L)) \end{aligned} \tag{1}$$

where $I_o$ is the output intensity, $I_i$ is the input intensity, $\beta = \frac{2\pi n_{eff}}{\lambda}$ is the propagation constant, $\lambda$ is the wavelength of light and $\Delta L$ is the path difference. We cannot easily vary the path difference of the MZI or effective index of the material in the PIC. However, we can vary the wavelength of the input light in the experiments. For variations in wavelength, we can use the above eq. 1 as a transfer function of the MZI as a function of the input wavelength of light [1]. This transfer function reads,

$$T(\lambda) = \frac{1}{2}\left(1+\cos\left(\frac{2\pi n_{eff}\Delta L}{\lambda}\right)\right) \tag{2}$$

For a given path difference $\Delta L$, if we vary phase difference of the MZI by varying the wavelength. We can modulate the output intensity from 0 to 1 in a periodic manner by linearly varying the wavelength as observed in a Fabry-Perot cavity. The free spectral range (FSR) of a MZI can be derived to be

$$FSR(\Delta L) = \frac{\lambda^2}{\Delta L n_g} \tag{3}$$

where $n_g = n - \lambda\frac{dn}{d\lambda}$ is the group index of the waveguide material.

These equations give us an understanding of what to expect from an ideal MZI. In the following section, we describe the numerical simulation results of a MZI.

## III. Simulation

Just like we use appropriate coatings on the beam splitters and mirrors for a given wavelength and characterize their absorption/reflection profiles for a free space MZI, we need to get an idea of how a non-ideal Y-brach and waveguide functions. For this we use simulations with material parameters of these components. Apart from the components of the MZI, we will also need to evaluate the performance of grating couplers that are used to inject the light in and out of the MZI during test and measurement.

Using Lumerical MODE's eigen mode solver, we simulate a Si slab waveguide that is 500 nm wide and 220 nm thick on a $SiO_2$ substrate and find a quasi-TE eigen mode of the waveguide for a wavelength of 1550 nm. Fig. 1 shows the intensity profile of this mode with colorbar in log scale. It can be seen that most of the intensity is contained with in the waveguide. By running wavelength sweeps on this simulation in Lumerical MODE, we obtained effective refractive index and group index as a function of wavelength. We then model the effective index as a polynomial function of wavelength $\lambda$

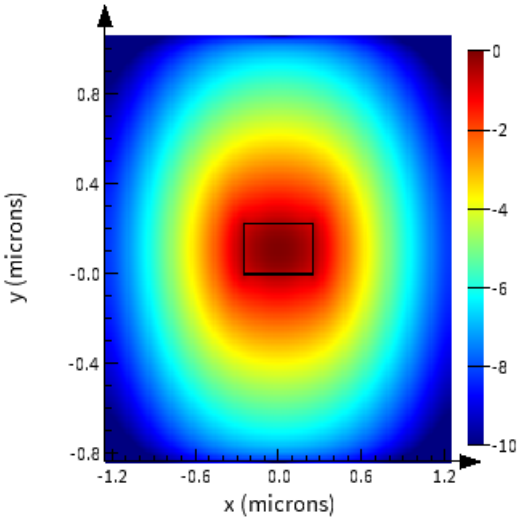


Fig. 1. Intensity of light in a quasi-TE eigen mode of the Si waveguide in a $SiO_2$ substrate. The black rectangle represents the boundary of the waveguide.

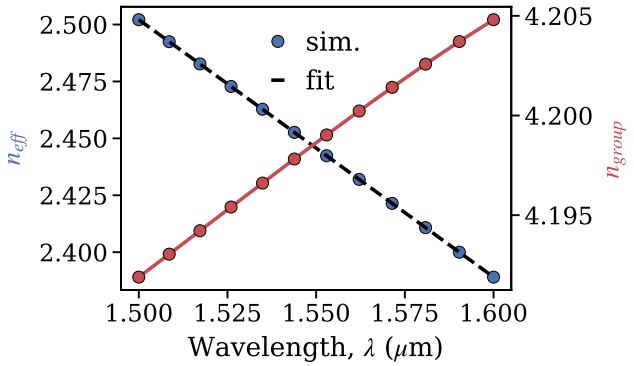


Fig. 2. Effective refractive index (blue dots) and group index of the waveguide (red dots) as a function of wavelength $\lambda$. The black dashed line is the polynomial fit as shown in eq. 4.

centered around the wavelength of interest 1.55 $\mu$m. The fit to the model is shown in Fig. 2 and the fit function reads,

$$n_{eff}(\lambda) = 2.446 - 1.131(\lambda - 1.55) - 0.042(\lambda - 1.55)^2 \quad (4)$$

We can use this model for the effective index of the waveguide in the simulation. We can also use a loss coefficient of 3 db/cm for propagation in the waveguide.

Using the Compact Model Library from the course management, MZI is simulated using Lumerical INTERCONNECT shown in Fig. 3 and the simulations results are summarized in Fig. 4. The red plain line represents the transmission power out of the grating coupler after the MZI. It should be noted that the transmission falls pretty fast as the wavelength varies. It can be considered that the band width of the device is about 40 nm. To understand this further, we simulate the trasmission from grating couplers to get an idea of their insertion loss. Figure 5 shows the insertion loss of a grating coupler and insertion loss of two grating couplers in series. It seems most of the loss in the MZI simulation seems to be due to the insertion

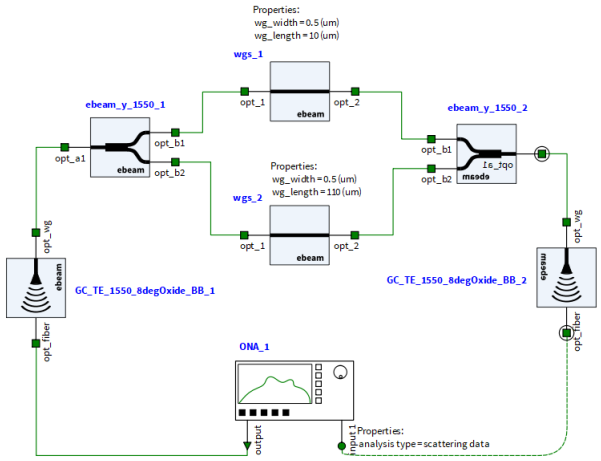


Fig. 3. Simulation of the MZI using the compact model library

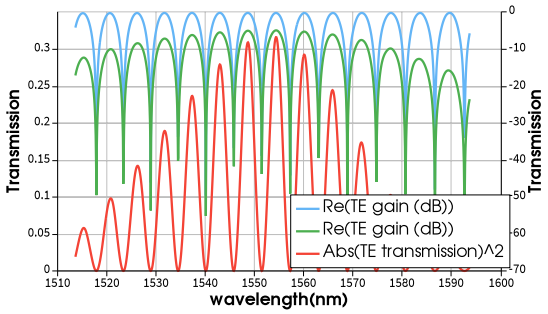


Fig. 4. Transmission of the simulated MZI for $\Delta L$=100nm. Blue and green plain line indicate the transmission gain in dB (ticks on the right hand side) with and without the grating couplers, respectively. Red line represents the transmission power. It should be noted that the transmission falls pretty fast as the wavelength varies. It can be considered that the band width of the device is about 40 nm.

loss of the grating couplers. This is also shown in difference between blue and green plain lines of Figure 4.

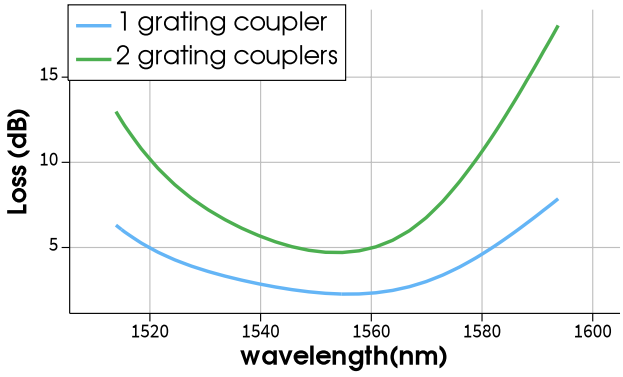


Fig. 5. Insertion loss of the grating coupler (plain blue line) used in the simulation. Green plain line shows the loss profile of two grating couplers in series.

| $\Delta L(\mu m)$ | FSR (nm) |
|---|---|
| 30 | 19.067460 |
| 60 | 9.533730 |
| 100 | 5.720238 |
| 150 | 3.813492 |
| 200 | 2.860119 |
| 300 | 1.906746 |

TABLE I
PROPOSED PATH LENGTH DIFFERENCES FOR MZIS VS ESTIMATED FSR.

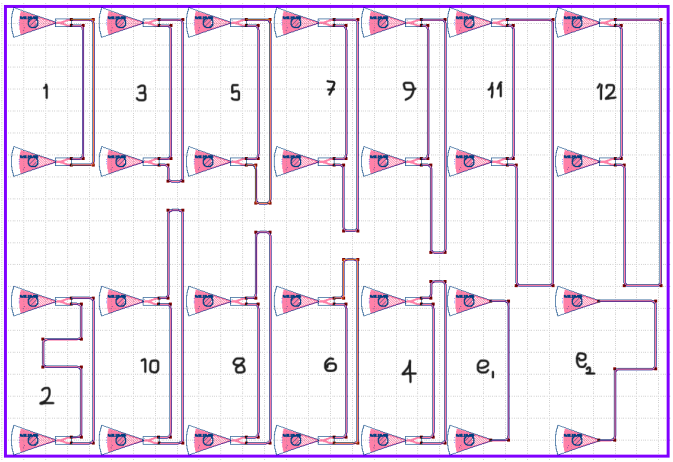


Fig. 6. Layout of the PIC with 12 MZIs proposed length differences of table I. Two devices $e_1$ and $e_2$ with just grating couplers connected with two different lengths of waveguides fabricated for de-embedding the data.

| Device | $\Delta L$ ($\mu$m) | $n_g$ | FSR (nm) |
|---|---|---|---|
| Set 1 | | | |
| MZI1 | 30 | 4.189 | 19.12 |
| MZI3 | 60 | 4.186 | 9.57 |
| MZI5 | 100 | 4.187 | 5.74 |
| MZI7 | 150 | 4.189 | 3.82 |
| MZI9 | 200 | 4.188 | 2.87 |
| MZI11 | 300 | 4.187 | 1.91 |
| Set 2 | | | |
| MZI2 | 30 | 4.207 | 19.04 |
| MZI4 | 60 | 4.187 | 9.56 |
| MZI6 | 100 | 4.187 | 5.74 |
| MZI8 | 150 | 4.188 | 3.82 |
| MZI10 | 190 | 4.187 | 3.02 |
| MZI12 | 300 | 4.189 | 1.91 |
| | | $n_g$ = 4.189(5) | |

TABLE II
SUMMARY OF DATA ANALYSIS RESULTS FOR TWO SETS OF MZIS. THE AVERAGE GROUP INDEX OBTAINED FROM MZIS IS $n_g = 4.189(5)$.

| Geometry (nm×nm) | $n_{eff}$ | $n_g$ | notation |
|---|---|---|---|
| 500×220 (nominal) | 2.4457 | 4.1986 | $n_g^{model}$ |
| 470×215.3 | 2.3744 | 4.2469 | |
| 470×223.1 | 2.4038 | 4.2556 | $n_g^{max}$ |
| 510×215.3 | 2.4423 | 4.1769 | $n_g^{min}$ |
| 510×223.1 | 2.4714 | 4.1840 | |

TABLE III
CORNER ANALYSIS FOR ESTIMATING THE EFFECT OF VARIATIONS IN GEOMETRY OF THE WAVEGUIDE ON THE GROUP INDEX.

## IV. DESIGN LAYOUT

As the objective of the design is to measure the group index of the waveguide using the FSR measurement, we need to choose the path length difference between the two arms of the interferometer in such a way that allows us to measure the FSR as accurately as possible. As the transmission falls rapidly with wavelength around the central wavelength, the measurement window of 50 nm should contain a few FSR. From the wavelength scan of our wave guide, we have an estimate of group index to be around 4.2. Assuming our experimental value to fall around this, we can estimate the minimum path length difference *i.e.,* $\Delta L^{min} = \lambda^2/(40 \times 10^{-9} \times 4.2)$ needed to at least observe two peaks in the spectrum. The value of $\Delta L^{min}$ for $\lambda = 1.55\mu$m is 14.3 $\mu$m. Having this value in mind, we propose path length differences in table I that allow for a measurement of FSR. Figure 6 shows the layout of the PIC where two copies of each MZI (1 through 12) with length differences shown in table I are prepared for fabrication. Two devices with just grating couplers connected with two different lengths of waveguides are also proposed for fabrication to help us account for the narrow bandwidth of the grating couplers used.

## V. RESULTS AND DISCUSSION

The transmission data of the MZIs from the layout in figure 6 has been obtained and processed through the de-embedding where losses related to the bandwidth of the two grating couplers used in the design have been removed. This is done using the transmission data from the devices $e_1$ and $e_2$. We take the average of the transmission data and fit it to a fourth order polynomial (see figure 9) and build a model for loss as a function of wavelength for the grating coupler. This is then subtracted from all the data. In addition to this, the data in the wavelength range of 1500 nm to 1520 nm have also been discarded due to lower signal to noise ratio of the measurement in this region. The deembedded data are then fit with the transfer function, $H(\lambda)$ shown in eq. 5 where effective refractive index $n_{eff}(\lambda) = n_1 + n_2(\lambda - \lambda_0) + n_3(\lambda - \lambda_0)^2$. The waveguide propagation loss $\alpha$ and overall offset in the data $\beta$ are included to have a total of five fitting parameters. The group index, $n_g = n_1 - n_2\lambda_0$ can be derived from these parameters.

$$H(\lambda) = 10\log\frac{1}{4}\left|\left(1+\exp\left(\frac{2\pi i n_{eff}(\lambda)\Delta L}{\lambda} - \frac{\alpha\Delta L}{2}\right)\right)\right|^2 + \beta \quad (5)$$

We divide the fabricated MZI devices into two sets which contain MZIs with length differences shown in table I. The results of the data analysis are summarized in table II. All the analyzed data with the fitting curves are plotted in the appendix. We can see that the experimental results are very close to the expectation values from simulations. We will verify if the mismatch is quantitatively within our fabrication capabilities. The fabrication process is known to have errors in the width and thickness of the waveguides. To account for the changes in geometry, we perform corner analysis using the known variations due to fabrication in the cross section of the waveguide. This is tabulated in table III. This gives us minimum ($n_g^{min}$) and maximum ($n_g^{max}$) bounds for $n_g$ that we can expect from the experimental data. The experimentally

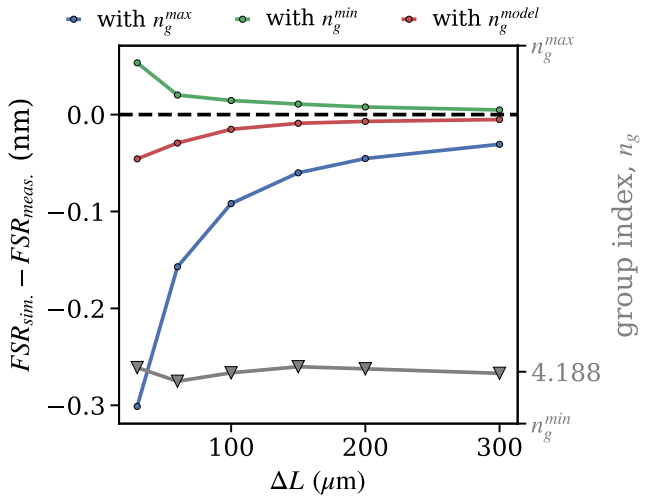


Fig. 7. The difference of FSR calculated with different group indices w.r.t to the measured FSR as a function of $\Delta L$ for MZIs Set 1.

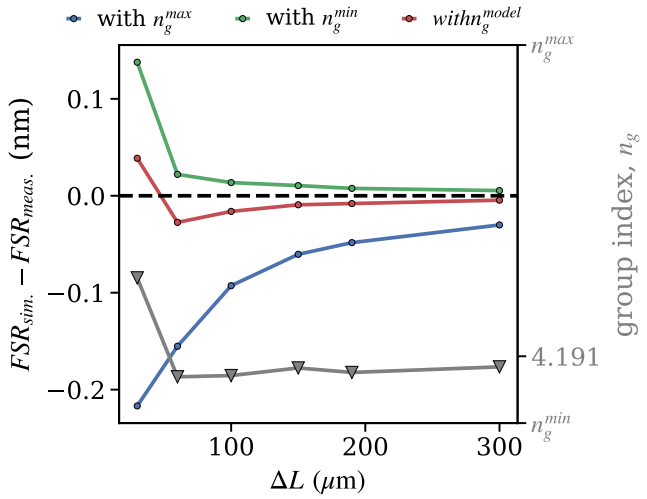


Fig. 8. The difference of FSR calculated with different group indices w.r.t to the measured FSR as a function of $\Delta L$ for MZIs Set 2.

determined value for $n_g = 4.189(5)$ lies with in these bounds shown in table III. We have also calculated the FSR for each set of MZIs with $n_g^{min}$, $n_g^{max}$ and $n_g^{model}$ and determined the difference w.r.t to the measured FSR. These values are plotted in figures 7 and 8 against length differences $\Delta L$. It is clear that the measured FSR lies in between the bounds set by the bounds of $n_g$ for all the devices.

## VI. Conclusion

In conclusion, the paper summarizes the basic theoretical ideas, design methodology and measurement analysis involved in designing a MZI on PIC. We have proposed various path length differences for MZI to measure the group index of our 500 nm $\times$220 nm Si slab waveguide on a $SiO_2$ substrate and we have successfully measured it and found it to be within the error bounds dictated by the fabrication capabilities.

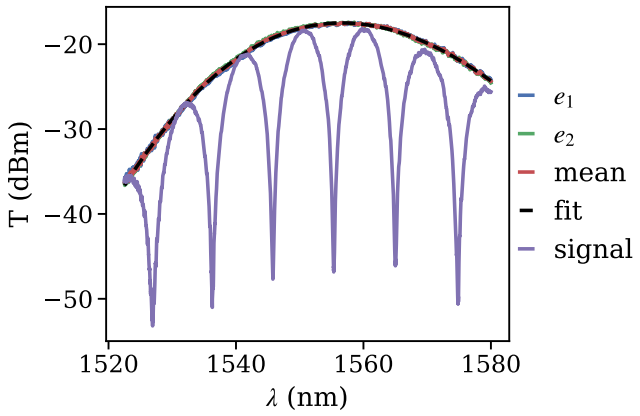


Fig. 9. Transimission data from the devices made for deembedding. Black dashed line represents the fit model that has been removed from the transmission data from all the MZIs. A sample signal is shown for reference.

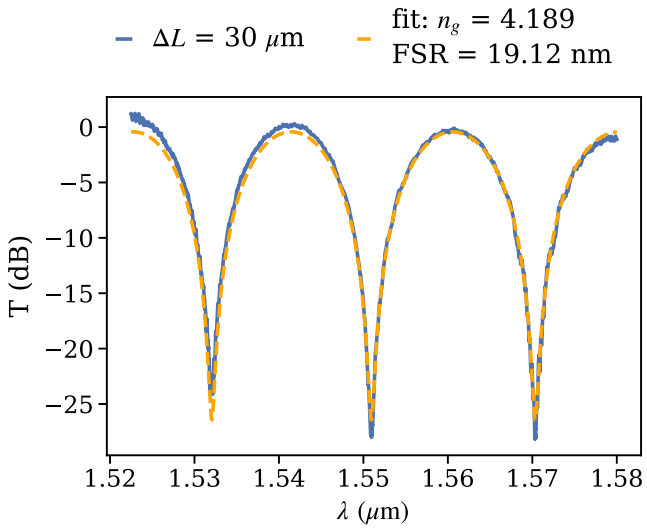


Fig. 10. Fitting of transmission data from MZI1 from layout shown in figure 6.

## References

[1] L. Chrostowski and M. Hochberg, *Silicon Photonics Design*. Cambridge University Press, 2015.

## VII. Appendix

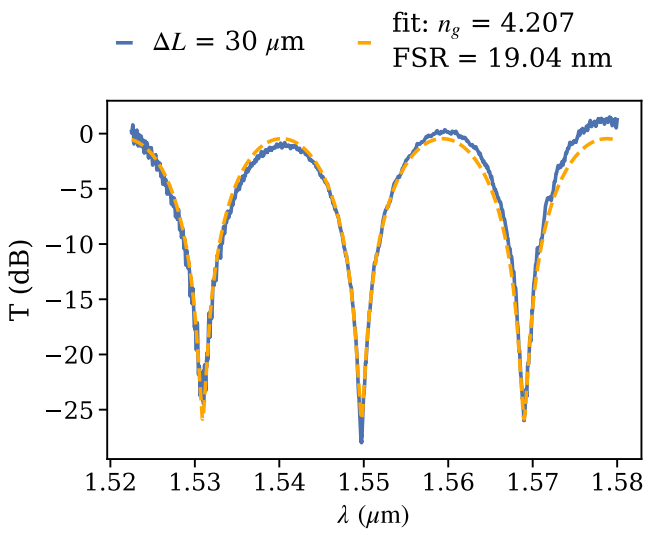


Fig. 11. Fitting of transmission data from MZI2 from layout shown in figure 6.

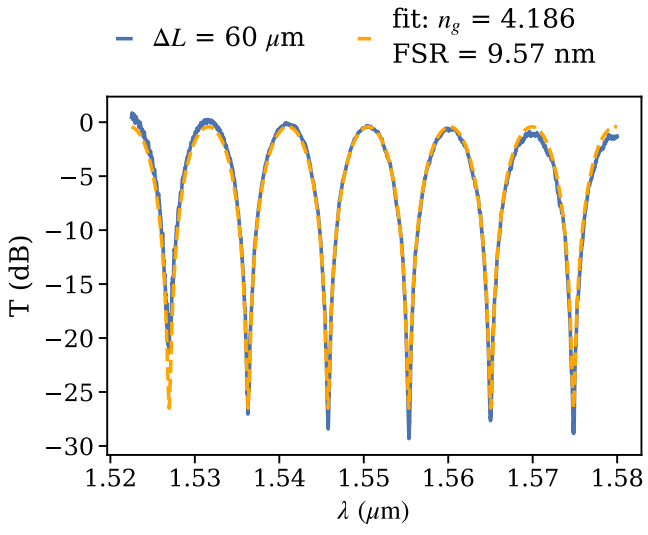


Fig. 12. Fitting of transmission data from MZI3 from layout shown in figure 6.

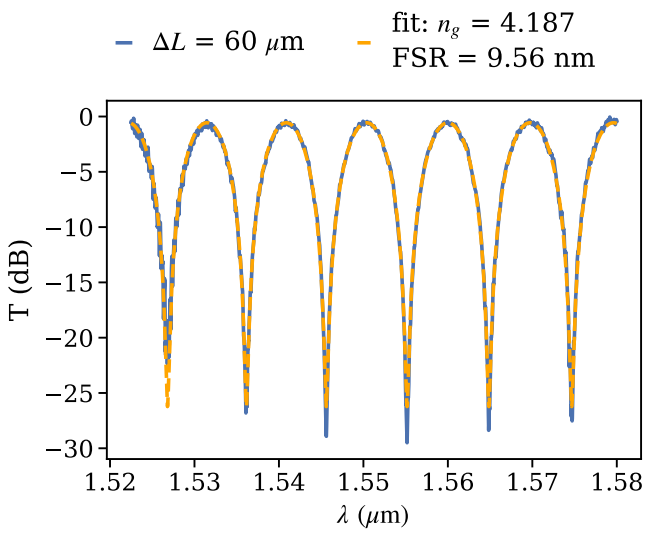


Fig. 13. Fitting of transmission data from MZI4 from layout shown in figure 6.

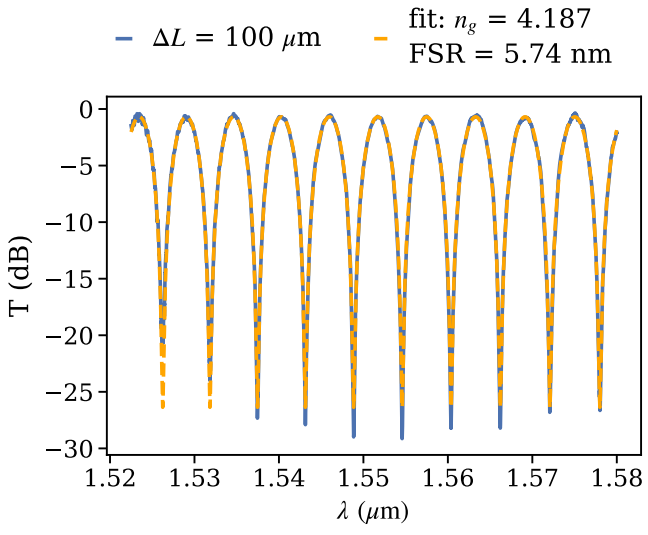


Fig. 14. Fitting of transmission data from MZI5 from layout shown in figure 6.

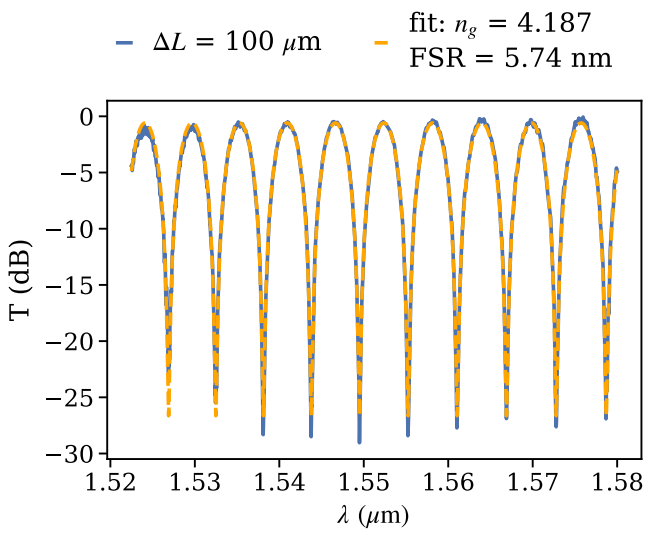


Fig. 15. Fitting of transmission data from MZI6 from layout shown in figure 6.

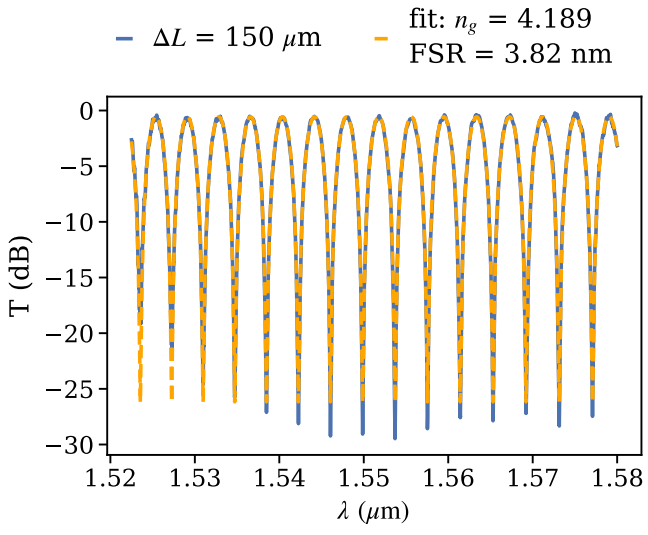


Fig. 16. Fitting of transmission data from MZI7 from layout shown in figure 6.

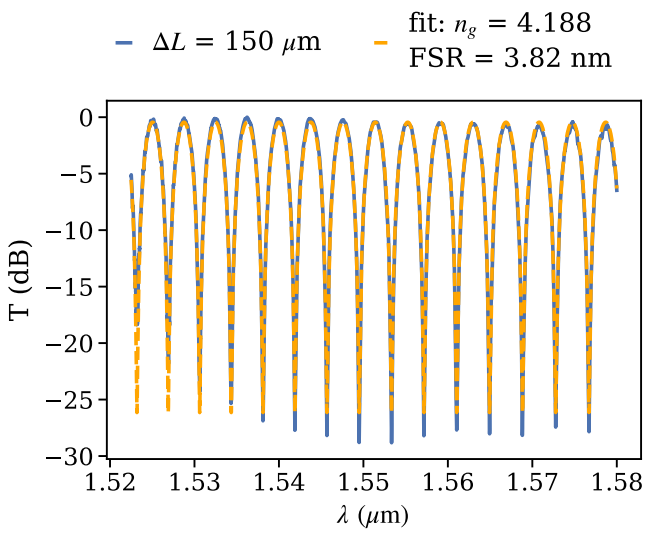


Fig. 17. Fitting of transmission data from MZI8 from layout shown in figure 6.

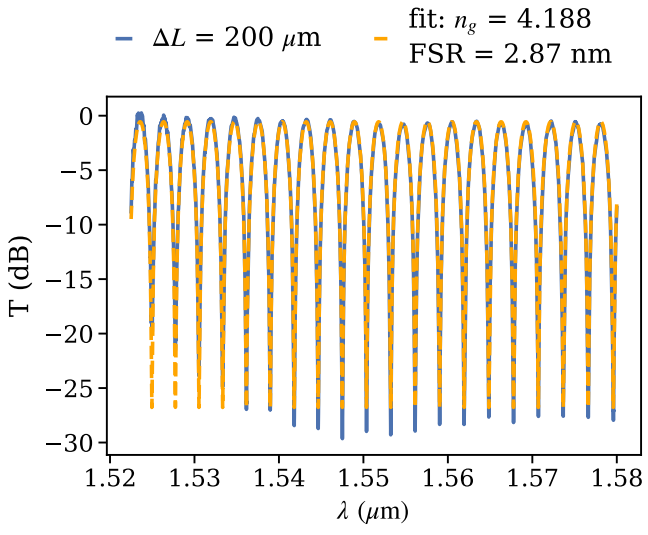


Fig. 18. Fitting of transmission data from MZI9 from layout shown in figure 6.

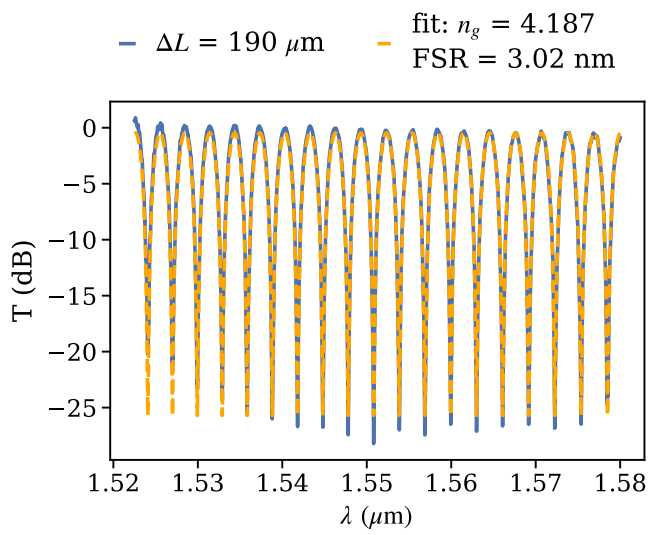


Fig. 19. Fitting of transmission data from MZI10 from layout shown in figure 6. This was supposed to be the second copy of the MZI with $\Delta L = 200$ $\mu$m. However, a mistake has been made in the layout.

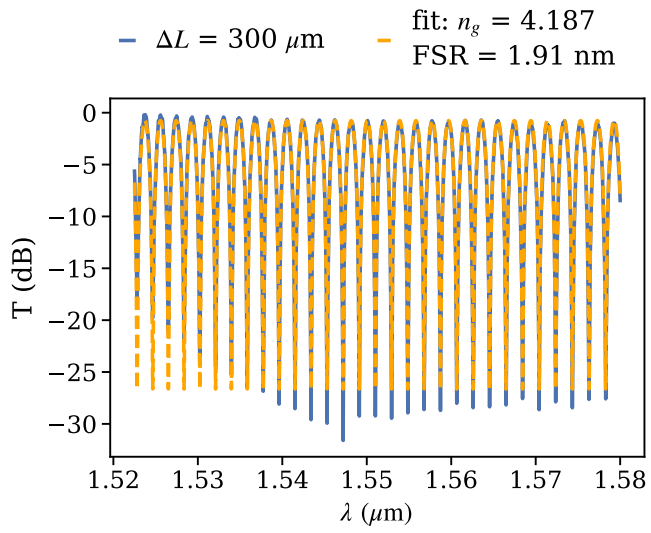


Fig. 20. Fitting of transmission data from MZI11 from layout shown in figure 6.

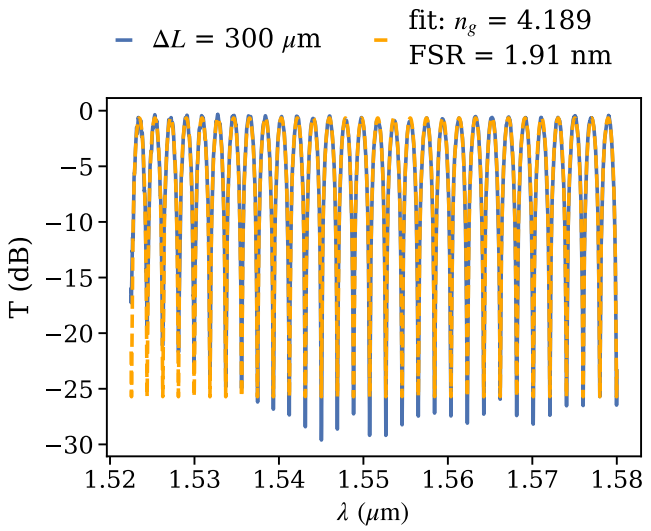


Fig. 21. Fitting of transmission data from MZI12 from layout shown in figure 6.